PHILOSOPHICAL TRANSACTIONS OF THE ROYAL SOCIETY A MATHEMATICAL, PHYSICAL & ENGINEERING SCIENCES

Internal Waves in JASIN [and Discussion]

M. D. Levine, C. A. Paulson, M. G. Briscoe, R. A. Weller, H. Peters, H. M. Van Aken, J. M. Huthnance, G. Siedler and E. D. R. Shearman

Phil. Trans. R. Soc. Lond. A 1983 **308**, 389-405
doi: 10.1098/rsta.1983.0011

Phil. Trans. R. Soc. Lond. A **308**, 389–405 (1983)
Printed in Great Britain

Internal waves in JASIN

By M. D. Levine†, C. A. Paulson†, M. G. Briscoe‡,
R. A. Weller‡ and H. Peters§
† *Oregon State University, Corvallis, Oregon* 97331, *U.S.A.*
‡ *Woods Hole Oceanographic Institution, Woods Hole, Massachusetts* 02543, *U.S.A.*
§ *Institut für Meereskunde an der Universität Kiel*, 23 *Kiel, F.R.G.*

The internal wavefield during the Joint Air–Sea Interaction (JASIN) experiment was monitored by moored current meters and moored and towed thermistor chains. The observations were concentrated in the upper ocean near the centre of Rockall Trough, but velocity measurements were also made near topographic features and throughout the water column. Observed spectra are compared with results from the deep ocean, as represented by the Garrett–Munk (GM) model of the spectral continuum, and are generally found to have spectral levels equal to or greater than the GM spectrum. The greatest deviation from the GM spectrum occurs at high frequencies and wavenumbers where the observed spectra often exhibit a spectral shoulder and high vertical coherence. These features, also found in other upper-ocean spectra, are explained by a model composed of three vertically standing modes. The spatial variation of internal wave variance is related to topography: variance is highest near rough topography. The ratio of variance in the semidiurnal tidal band to variance in a band in the continuum is approximately constant. The possibility of a dynamical link between the two frequency bands requires further investigation. The semidiurnal internal tide varies temporally and spatially. Rockall Bank is identified as the source of an energetic beam of tidal oscillations during a one-week period.

1. Introduction

The oceanic internal wavefield can be divided into four régimes according to frequency: spectral continuum, high frequency band, tidal band and near-inertial band. The spectral continuum refers to internal waves that can be described statistically as a sum of random waves having a continuum of frequencies and wavenumbers. This is the assumption of the Garrett–Munk (GM) internal wave model (Garrett & Munk 1972, 1975). The GM model gives a consistent description of the internal wavefield in the deep ocean which agrees with observations. The high frequency band includes waves at frequencies preceding the final spectral cut-off. This band is distinguished from the continuum by a spectral peak or shoulder and high coherence. Internal waves at semidiurnal tidal frequency are generated by interaction of the barotropic tide with topography (see review by Hendershott 1981). The tidal peaks are superimposed on the background continuum spectrum and represent a significant fraction of the total internal wave variance. For comprehensive discussions of internal waves and reviews of recent research, the reader is referred to papers by Garrett & Munk (1979), Gregg & Briscoe (1979) and Munk (1981). The properties of the near-inertial band are discussed by Weller & Halpern (this symposium).

The objectives of this paper are to describe observations of internal waves made during the Joint Air–Sea Interaction (JASIN) experiment and to compare the observations with models and the results of other experiments. The observations used are horizontal velocity from moored

current meters and vertical isotherm displacement from moored and towed thermistor chains. The observations were concentrated in the upper ocean of the Rockall Trough west of Scotland; however, some measurements were as deep as 1500 m. Spectra of velocity and vertical displacement are compared with the GM model, which is a good representation of observations in the deep ocean away from topography. We might expect deviations from GM spectra in the upper ocean where vertical density gradients are larger and more variable than below and where there are unique processes, which may generate, modify or dissipate internal waves. A

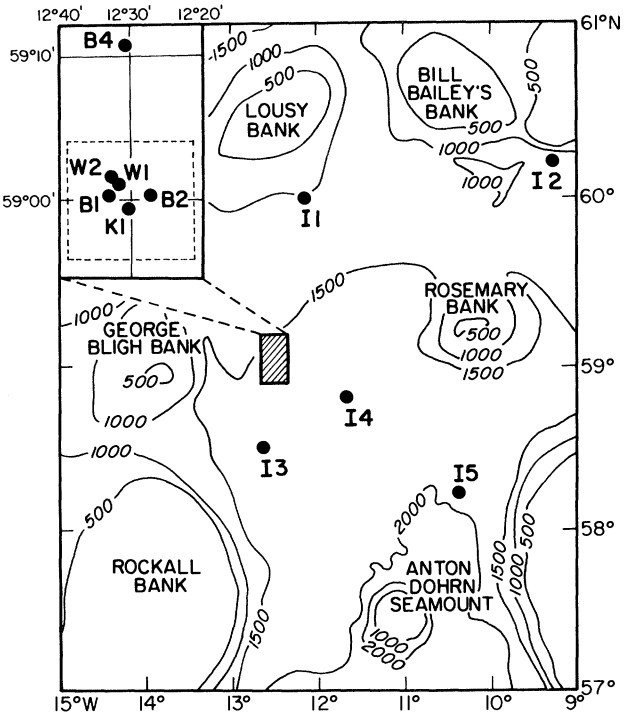

FIGURE 1. Mooring locations. The thermistor-chain tow track is indicated by a dashed line in the inset at upper left corner. Depth contours are labelled in metres.

large deviation from the GM model in the high frequency band is modelled by a sum of three vertical modes. The validity of the three-mode model is evaluated by comparison with observed spectra and vertical coherences. The analysis of one week of observations of the semidiurnal internal tide is summarized. The spatial variability over the JASIN area of the internal tide and the internal wave continuum is also described. The spectral level of the continuum is compared with the magnitude of the internal tide and with the GM level. Finally, spectra and coherences are compared with upper-ocean observations in the Mixed Layer Experiment (MILE) and the Global Atmospheric Research Project Atlantic Tropical Experiment (GATE).

2. OBSERVATIONS

The observations of internal waves come from a variety of instruments distributed throughout the JASIN area (figure 1). Measurements of internal waves in the Fixed Intensive Array (FIA) were taken at moorings B1, B2 and B4 by Aanderaa thermistor chains (deWitt *et al.* 1980), at moorings W1 and W2 by vector-averaging current meters (VACM) and vector-measuring current meters (VMCM) (Tarbell *et al.* 1979), and on tracks around the FIA by a thermistor chain

towed from a ship (Baumann *et al.* 1980). Internal wave data on larger spatial scales were recorded by Aanderaa current meters on the five I moorings (Gould *et al.* 1983). Vertical profiles of the density field and the corresponding buoyancy or Väisälä frequency, concentrated around the FIA, were taken with a Neil Brown Instrument Systems' conductivity–temperature–depth (CTD) profiler from R.V. *Atlantis*-II (Pennington & Briscoe 1979).

There were two thermistor chains on each of the B moorings. The upper chains measured

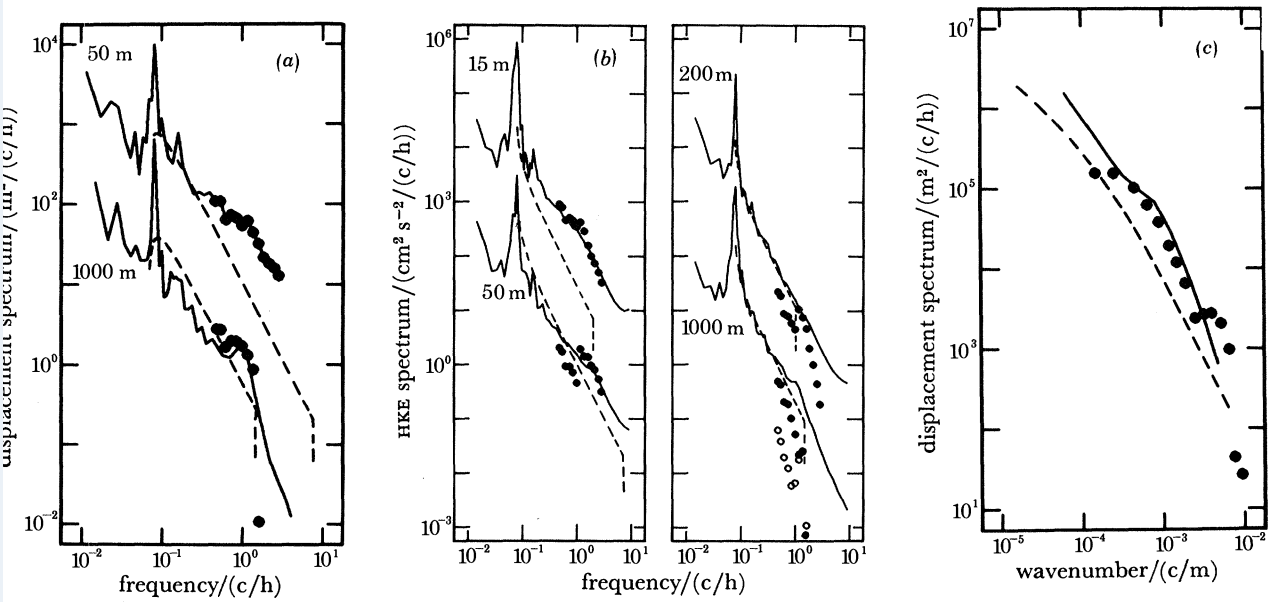

FIGURE 2. Observed average spectra (solid line) are shown along with the GM model (dashed line) and the three-mode model (solid symbols). (*a*) Frequency spectra of vertical displacement from B1 at 50 m (offset by 10^2) and from W1 at 1000 m. (*b*) Frequency spectra of HKE from W2 at 15 m (offset by 10^2) and 50 m and W1 at 200 m (offset by 10^2) and 1000 m. At 1000 m the two-mode model is indicated by open symbols. (*c*) Wavenumber spectrum of vertical displacement from thermistor-chain tows at an average depth of 50 m.

temperature at 11 depths from 5 to 35 m at separations of 3 m; the 10 sensors on the deep chains were spaced every 5 m from 37 to 82 m. The interval between samples was 10 min. Depths of isotherms were computed as a function of time by linear interpolation between adjacent sensors. The frequency spectrum of isotherm depth calculated from the entire 40 day time series is shown in figure 2*a* (deWitt *et al.* 1980).

The velocity at W1, supported by a subsurface float, was measured with VACMS sampling at 32 times per hour and spaced every 3 m from 79 to 124 m as well as at 195, 200, 210, 295, 300, 310 and 1000 m. On the surface-floated W2 mooring, 8 VMCMS, sampling at 30 times per hour were distributed from 10 to 85 m. Representative spectra of the 40 day time series are displayed in figure 2*b* as horizontal kinetic energy (HKE); they are formed by taking half the sum of the spectra of the north and east components (Tarbell *et al.* 1979).

The towed thermistor chain had sensors at 2 m intervals from 20 to 70 m and was towed by by the *Atlantis*-II at about 3 m s^{-1}. The four tows that are considered here each consisted of two circuits around a square 15 km $\times$ 15 km centred in the FIA. The temperature observations were low-pass filtered by computing sequential 30 s averages, which effectively removed variations caused by surface gravity waves and ship heave. Isotherm depths were then determined by linear interpolation between measurements at adjacent depths. Horizontal wavenumber

spectra were calculated from isotherm depths along each straight side of the square by use of the average tow speed to convert from temporal to spatial sampling. Ensemble-averaged spectra of all sides are shown in figure 2*c* (Baumann *et al.* 1980).

A mean buoyancy frequency profile was computed from 17 CTD casts made within 15 km of the W moorings (figure 3) (Pennington & Briscoe 1979). This profile is taken as representative of the JASIN region and is used in interpreting and scaling all the internal wave measurements.

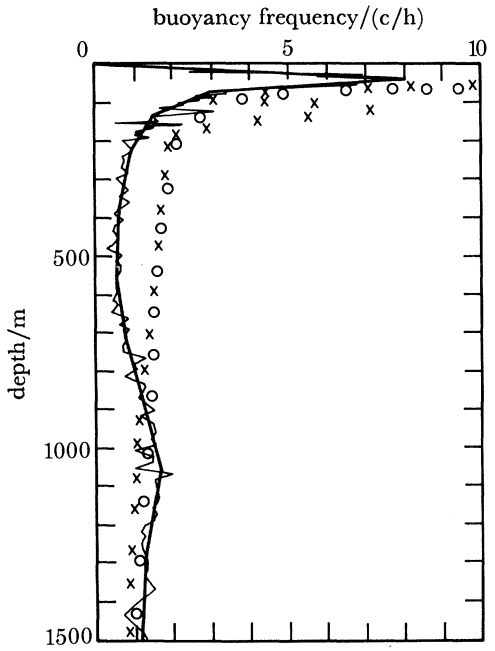

FIGURE 3. Mean buoyancy frequency profile from JASIN (thin line) (Pennington & Briscoe 1979). Bold line indicates the approximation used in solving for vertical wavefunctions. Mean profiles from GATE (circles) (Käse & Siedler 1980) and from MILE (crosses) (Levine *et al.* 1982) are also shown.

3. SPECTRAL CONTINUUM

The spectral continuum in the deep ocean away from the equator and topography is well represented by the GM model (Wunsch 1976; Wunsch & Webb 1979). The GM model is therefore a useful framework for comparison of internal waves in different environments. Some comparisons of the GM model with other upper-ocean data are now available (Roth *et al.* 1981). One goal of the comparisons is to determine universal characteristics of the internal wavefield in the upper ocean. The JASIN measurements can contribute toward this goal.

The GM model of the spectrum, as formulated by Desaubies (1976), will be used as a reference. The spectra of vertical displacement and HKE as a function of frequency ω and the spectrum of vertical displacement as a function of horizontal wavenumber k (asymptotically valid at high wavenumber) are given respectively by

$$S_\xi(\omega) = \frac{2}{\pi} r \frac{f}{N(z)} \frac{(\omega^2 - f^2)^{\frac{1}{2}}}{\omega^3}, \tag{1}$$

$$S_{\mathrm{HKE}}(\omega) = 4\pi r f N(z) \frac{(\omega^2 + f^2)}{\omega^3 (\omega^2 - f^2)^{\frac{1}{2}}}, \tag{2}$$

$$S_\xi(k) = \left(\frac{2}{\pi}\right)^3 rt \frac{f}{N(z)} \left(\ln \frac{N}{f} - \frac{N^2 - f^2}{2N^2}\right) \frac{1}{k^2}, \tag{3}$$

where f and N are the inertial and buoyancy frequency respectively. Frequency and wavenumber are expressed in cycles per hour (c/h) and cycles per metre (c/m) respectively. The four parameters of the GM model, E, energy level; j, effective mode number; b, vertical depth scale of N; and N_0, buoyancy frequency scale, have been rewritten as two parameters, $r = Eb^2N_0$ and $t = j/2bN_0$. The values of $r = 190\ \mathrm{m^2\ c/h}$ and $t = 4.2 \times 10^{-4}$ (c/m)/(c/h), determined from deep-ocean (Internal Wave Experiment) IWEX data as reported by Roth *et al.* (1981), are used in the comparisons described subsequently.

Frequency spectra of isotherm displacement measured from B1 and W1 at depths of 50 and 1000 m respectively are plotted with the GM model (1) in figure 2*a*. Vertical displacement is estimated at 50 m by following the depth of an isotherm with the thermistor chain at B1 and at 1000 m by assuming a constant vertical temperature gradient of 0.0058 K/m derived from CTD profiles (Pennington & Briscoe 1979). At 50 m the shape of the observed spectrum is quite different from the GM model everywhere in the internal wave frequency band. The greatest deviation occurs at high frequency where the observed spectrum is nearly ten times the GM spectrum. At 1000 m the slope of the model and observed spectra are similar below 0.3 c/h though the model is twice the observed spectrum. At higher frequency the observed spectrum has a pronounced peak not present in the model. Although temperature was measured at other depths, vertical displacement cannot be inferred because of the large variability of the mean gradient.

Frequency spectra of HKE are compared with the GM model (2) in figure 2*b*. The spectral shape agrees fairly well at low frequencies. However, above 0.5 c/h the observed spectral slope is generally less steep than the ω^{-2} of the GM model except at 200 m depth where no change of slope is evident.

The horizontal wavenumber spectrum of isotherm displacement measured at 50 m agrees favourably with GM levels (3) at low wavenumber (*ca.* 10^{-4} c/m, figure 2*c*). At higher wavenumbers the observed spectrum deviates positively from the deep-ocean levels, forming a shoulder at *ca.* 10^{-3} c/m.

In general the levels of the observed spectra agree with the GM levels at low frequency and wavenumber. The greatest exception occurs at 50 m where the observed HKE and displacement frequency spectra are both one half to one third the GM levels. This discrepancy cannot be explained by the uncertainty in the value of N used in the model since the displacement spectrum scales with N, (2), and the HKE spectrum scales with $1/N$, (3). Hence, a value of N that would improve agreement with the displacement spectrum would worsen agreement with the HKE spectrum and vice versa. At high frequency and wavenumber the observed spectra usually exhibit a spectral shoulder where the spectral slope is less steep and the spectral level is higher than the GM level.

4. High frequency and wavenumber

The JASIN internal wave spectra deviate significantly from the GM model of the continuum at high frequency and wavenumber. Not only is there usually a spectral peak or shoulder but also there is high vertical coherence in both vertical displacement and velocity from 0.5 to 3.0 c/h and from 5×10^{-4} to 20×10^{-4} c/m (figure 4). High vertical coherence at a given frequency indicates that either there are only a few statistically uncorrelated waves of different wavenumbers (modes) or there are many modes present that are highly correlated. Here

PHILOSOPHICAL TRANSACTIONS OF THE ROYAL SOCIETY A MATHEMATICAL, PHYSICAL & ENGINEERING SCIENCES

a simple model with the assumption of a few uncorrelated waves is constructed and compared with the data.

Assume the high frequency wavefield is composed of a sum of linear random waves that propogate horizontally with an isotropic distribution and are vertically standing. The spectra can then be written (based on Willebrand *et al.* 1977):

$$\tilde{S}_\xi(\omega) = \sum_n E_n(\omega)\psi_n^2(\omega, z), \tag{4}$$

$$\tilde{S}_{\mathrm{HKE}}(\omega) = \sum_n \frac{\omega}{2}\left(\frac{\omega^2+f^2}{k_n^2}\right) E_n(\omega)\left(\frac{\partial\psi_n}{\partial z}\right)^2, \tag{5}$$

$$\tilde{S}_\xi(k) = \frac{2}{\pi}\sum_n \int_{\omega_n}^{\infty} \mathrm{d}\omega\, E_n(\omega)\,\psi_n^2(\omega,z)(k_n^2(\omega)-k^2)^{-\frac{1}{2}}, \tag{6}$$

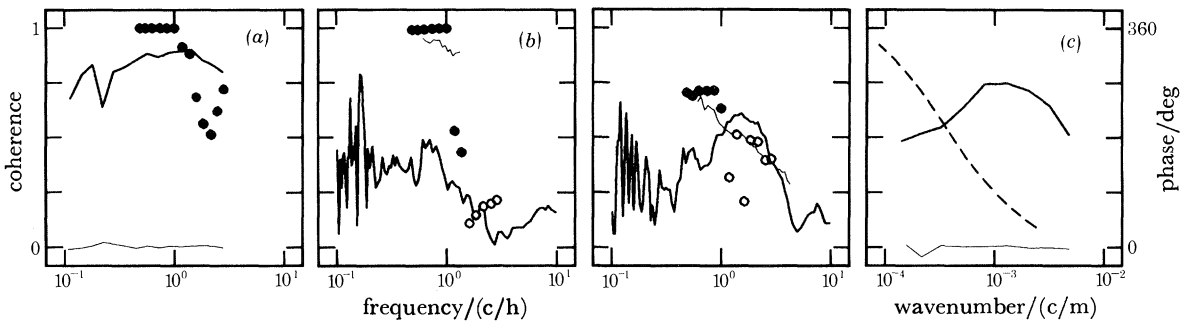

FIGURE 4. Observed vertical coherence (bold line) and significant phase (thin line) are shown along with coherences of the three-mode model (solid symbols, in phase; open symbols, 180° out of phase). (*a*) Frequency coherence between isotherms from B1 at average depths of 45 and 59 m. (*b*) Frequency coherence of clockwise rotary velocity components on W2 between 10 and 40 m and 10 and 85 m. (*c*) Wavenumber coherence between isotherms from thermistor-chain tows with an average vertical separation of 25–30 m regardless of actual mean depth. GM model coherence is indicated by dashed line.

where ω_n is defined by $k_n(\omega_n) = k$; the vertical structure of the modes is given by the solution of the eigenvalue problem

$$\frac{\partial^2\psi}{\partial z^2} + k^2\frac{N^2(z)-\omega^2}{\omega^2-f^2}\psi = 0, \quad \text{where } \psi(0) = \psi(-\mathrm{H}) = 0 \tag{7}$$

and $k = k_n(\omega)$ is the dispersion relation. The vertical mode representation is used rather than the WKB approximation because N is not a slowly varying function of depth in the upper ocean. To determine the number of modes to be included in the model, the dispersion curves were calculated numerically for $N(z)$ as given in figure 3 and are plotted as horizontal phase velocity ω/k against frequency (figure 5). In regions where the mean flow becomes equal to the phase velocity, the nonlinear advective terms become important in the momentum balance. Motions at near-interial and tidal frequency are of low enough frequency to appear as steady flow to the high frequency waves and are fast enough (10–20 cm s^{-1}) to permit significant nonlinear interaction by the mechanism of critical layer absorption with internal waves travelling at low phase speeds (Munk 1981). This interaction will modify the vertical structure of the wavefield by preventing the establishment of free waves of high mode. Therefore the model is restricted to the three lowest modes.

PHILOSOPHICAL TRANSACTIONS OF THE ROYAL SOCIETY A MATHEMATICAL, PHYSICAL & ENGINEERING SCIENCES

It is assumed that the observed spectrum of vertical displacement from B1 at a depth of 50 m is a good measure of the high frequency internal waves. The spectrum of vertical displacement is chosen as a reference because the velocity spectrum is more subject to contamination by non-internal wave noise at high frequency (Müller *et al.* 1978). The model is forced to fit precisely the displacement spectrum at 50 m in the band 0.5–3.0 c/h where the high vertical coherence indicates dominance by a few modes. Model velocity and displacement spectra at other depths can then be calculated by use of (4)–(6) and compared with measurements from the nearby W moorings.

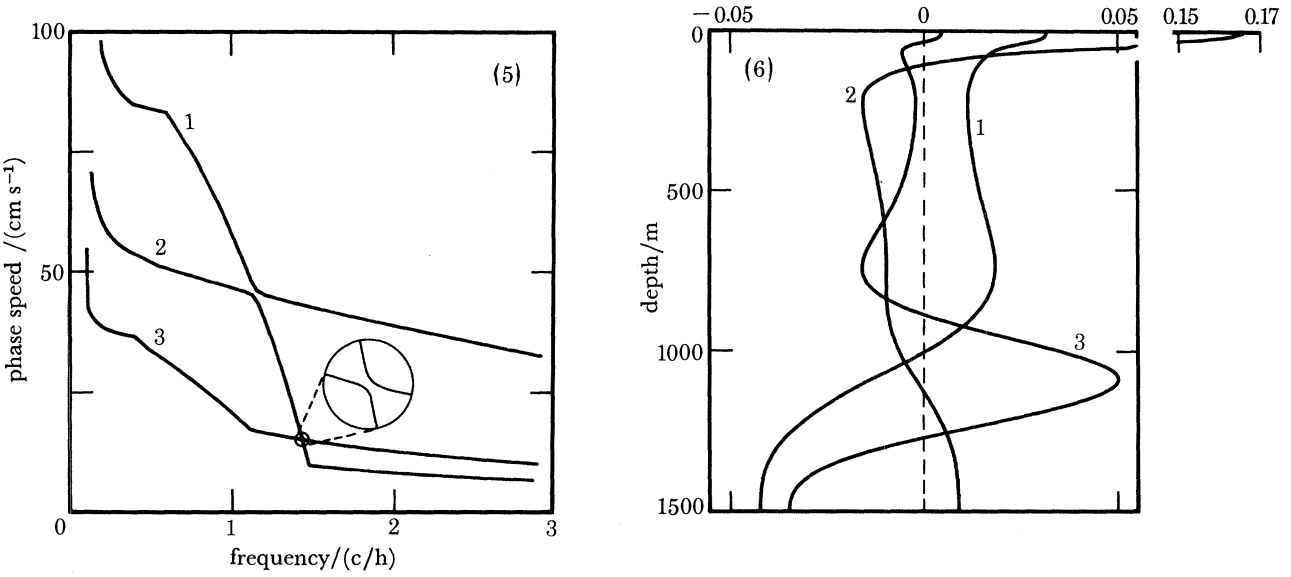

FIGURE 5. Dispersion curves displayed as horizontal phase speed (ω/k) against frequency (ω) for modes 1–3.
FIGURE 6. The first three vertical modes of horizontal velocity calculated from equation (7) by using the mean buoyancy frequency profile (figure 3).

A single-mode model of either mode 1 or mode 2 was tried and it did reproduce some of the features of the data. However, a better representation is obtained with a mixture of the two modes. For simplicity it was assumed that the vertically integrated energy (kinetic + potential) at each frequency is composed equally of the first two modes, i.e. $E_1 = E_2$. While this may not give the best fit possible, it does explain many of the observed features.

The greatest failure of the two-mode model occurs at 1000 m (figure 2*b*), where the level of the model is too low by a factor of 20. The reason is that for frequencies between 0.5 and 1.0 c/h there is a zero-crossing of mode 1 near 1000 m and mode 2 is small everywhere below 200 m (figure 6). Mode 3 has the opposite behaviour to mode 2 in this frequency band with relatively high values at depth and small-amplitude oscillations near the surface. Hence, mode 3 is a dominant mode in deep water and can be added to the model with little effect in the upper ocean. By including just 20% of mode 3, and retaining equal proportions of modes 1 and 2, the level of the 1000 m HKE spectrum is dramatically increased.

The model HKE spectra at other depths are plotted with the data in figure 2*b*. Features worth noting include:

(i) The shape and level of the three-mode model are in good agreement with the observed spectrum at 15 m. The GM curve is one tenth the observed spectrum at 1 c/h.

(ii) At 50 m the model mimics the observed spectral shoulder above 1 c/h; the GM curve is one third to one half the observed spectrum in this frequency band.

(iii) At 200 m the model indicates that the spectral cut-off should be above the 1.1 c/h given by local N. This is more consistent with the observed spectrum than the GM model although no clear cut-off is indicated.

(iv) The agreement at 1000 m is still not very good even with mode 3 added, but it is only slightly worse than the GM model. The presence of a shoulder at 1 c/h remains a mystery.

The spectrum of vertical displacement measured at 1000 m is also compared with the model (figure 2*a*), and the agreement between data and model is good. The model correctly indicates a spectral peak at *ca.* 1 c/h followed by a rapid spectral roll-off, while the GM level is too high at low frequency and too low at high frequency.

The model is also compared with the wavenumber spectrum of vertical displacement from horizontal tows of the thermistor chain around B1 and B2. Frequency spectra calculated over shorter time-segments encompassing the tows were used as a basis for comparison. The model spectrum (6), based on the averaged spectra from B1 and B2 during 22 August–6 September, is compared with the spectrum averaged from the four tows made during the same period (figure 2*c*). The agreement in both shape and level is remarkably good between 2×10^{-4} and 20×10^{-4} c/m. Below this range the model is lower than the observed spectrum because the model omits waves from below 0.5 c/h. There may be significant contributions to these low wavenumbers from frequencies below the highly coherent frequency band that have not been included.

Many of the sharp features in the model spectra, such as the jumps in the HKE spectra at 1 c/h at 50 and 200 m and the peaks in the wavenumber spectra at high wavenumber, would tend to be smoothed out if effects of the low frequency velocity field were included. Doppler shifting of the high frequency by the mean and low frequency currents would cause the energy of a wave at a given frequency to be smeared to both higher and lower frequencies, thereby filling in valleys and rounding peaks in the model spectrum. Mean and low frequency vertical shear would also affect the model results by modifying the vertical mode shapes (Peters 1982). The structure of the mode would then be a function of the propagation direction relative to the shear. A valley in a spectrum caused by a zero-crossing of a mode would tend to be smeared out in a wavefield composed of waves coming from many horizontal directions.

The vertical coherences calculated from the three-mode model are shown with observations in figure 4. Coherence estimates are very sensitive to non-internal wave signals so the model and data can only be compared qualitatively. The measured vertical coherence of displacement has a peak in the 0.5–3.0 c/h frequency band with a phase of zero. The model coherence between 35 and 50 m is consistent with these observations (figure 4*a*). The velocity coherences are also high in this range. Examination of the corresponding phase spectra at these frequencies indicates a phase near zero between 10 and 40 m and significant non-zero phase between 10 and 85 m (figure 4*b*). The model coherence and phase between 10 and 40 m is high and near-zero respectively at frequencies below the rapid roll-off at 1.5 c/h. Above 1.5 c/h the model coherences are small, consistent with the observations. Between 10 and 85 m the high coherence peak is evident in the model with the phase changing from 0° to 180° above 1 c/h. The observations indicate a phase of 180°; however, there are many complicating factors that will tend to alter this simple result. For example, the energy partition among the modes may not be steady in time. Then the dominant mode may change from one that is in phase between two depths to one that is 180° out of phase resulting in an average phase between 0° and 180°.

This may partly explain the observed phases. The wavenumber coherence between isotherms separated vertically by 10–15 m is shown in figure 4*c*. The GM level as given by Desaubies (1976) is shown for comparison. There is a high coherence peak at high wavenumber not given in the GM model that is apparently related to the high coherence peak in frequency (Katz & Briscoe 1979). From the dispersion relation, the high coherence in frequencies over 0.5–3.0 c/h corresponds in wavenumber space to wavenumbers *higher* than 2×10^{-4} c/m encompassing the range of the observed high coherence peak. The uncertainty in relating frequency to wavenumber occurs because the tow resolves only one component of the horizontal wavenumber vector.

5. Internal semidiurnal tide

The energy of the semidiurnal internal tide was a significant fraction of the total internal wave variance as demonstrated by the large peaks in the velocity and vertical displacement spectra (figure 2). A large portion of this tidal signal must have been due to the internal tide because large vertical displacements are nearly absent in the barotropic tide. Also, as will be shown in §6, there were large vertical variations of tidal velocity that indicate strong baroclinic motions.

During a one-week period, 22–29 August, large vertical displacements at tidal frequency were present at all three B moorings. Because of the relatively high horizontal and vertical coherence during this time, an analysis of the internal tide as a deterministic signal was performed (deWitt *et al.* 1982). The three displacement series filtered by two-hour running averages are shown in figure 7*a*. The series from B1 and B2 are nearly in phase while B4 is almost 180° out of phase. This indicates that the wave propagated nearly north–south with a half wavelength approximately equal to the distance between B1 and B4.

An analysis with the three moorings as an antenna indicates the time series are consistent with a plane wave of amplitude 10 m and wavelength 36 m, which propagated from either 25° or 155° west of north. Other plane-wave solutions (aliases) are possible, but they occur at higher wavenumbers and are therefore considered unlikely. A 36 km wavelength corresponds to a solution of (7) for mode 3; the wavelengths of modes 1 and 2 are 94 and 52 km respectively.

The measurements of vertical displacement from towed observations help resolve the ambiguity of the direction of propagation. The plane-wave solutions derived from the B moorings are compared with towed observations of vertical displacement taken around B1 and B2 (figure 1). The predicted displacements for a wave from the northwest and from the southwest are plotted with the low-passed data from a pair of east–west tracks (figure 7*b*, *c*). The agreement is obviously better with the wave travelling from the southwest, presumably from Rockall Bank. The time between the two east–west tows is *ca.* six hours or half a tidal period. The two tows nearly coincided with a maximum (figure 7*b*) and a minimum (figure 7*c*) tidal displacement.

The conclusion that the tide was generated from Rockall Bank is consistent with the effectiveness of topography in generating internal tides from barotropic tides. The effectiveness of topography can be determined by comparing the slope of the topography with the slope of the characteristic of the internal tide. The most effective generator is one with the slope of the topography greater than the slope of the characteristic (Baines 1974). Rockall Bank has a

PHILOSOPHICAL TRANSACTIONS OF THE ROYAL SOCIETY A MATHEMATICAL, PHYSICAL & ENGINEERING SCIENCES

slope greater than the characteristic from 400–1400 m depth, which indicates that it is an effective generator of the internal tide. There is no efficient generator to create waves from the northwest. Although the tide appears as a plane wave locally, on larger scales a beam-like pattern will be observed if a few of the low modes are correlated (deWitt *et al.* 1982). A schematic representation of the beam of high tidal energy generated from Rockall Bank is shown in figure 8. This theoretical beam structure is compared with tidal velocity variances measured from the W and I moorings over the same period. The qualitative agreement is good. Regions

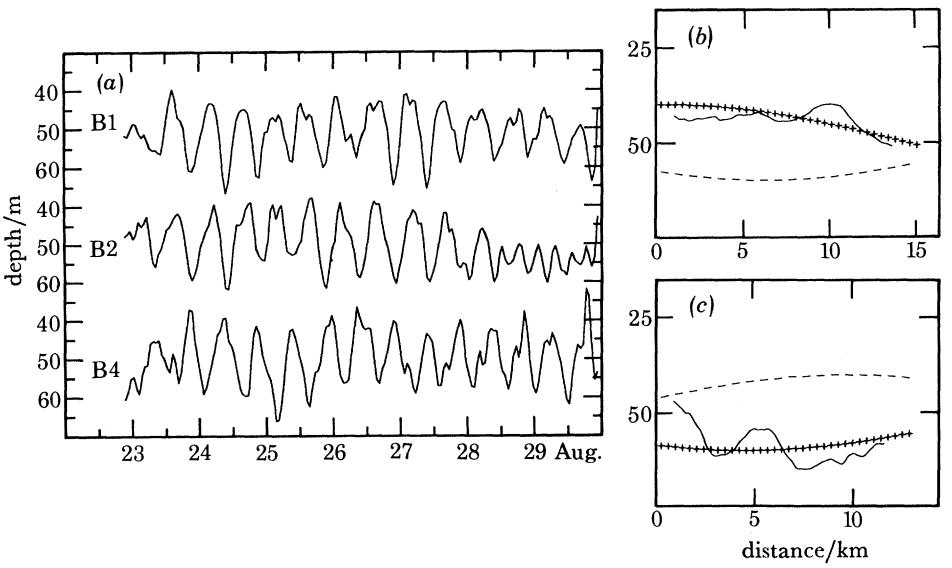

FIGURE 7. (*a*) Vertical displacement time series from B1, B2 and B4 (low-pass filtered). Note that B1 and B2 are nearly in phase while B4 is nearly 180° out of phase. (*b*) Vertical displacement from east–west tow track on 25 August. Based on the B array antenna, the fits of a plane wave from the southwest (+ + +) and from northwest (– – –) are shown. (*c*) Same track as (*b*) repeated *ca.* 6 h later. (From deWitt *et al.* 1982.)

of high tidal velocity variance are located within the beam; low variances are at the edge or outside the high energy beam. The beam structure was calculated on the assumption that the buoyancy frequency was constant in time and uniform horizontally. Variations in the density and velocity field in time and space associated with mesoscale features could cause a shifting of the beam pattern and be responsible for some of the observed variability. Dynamic interaction of the internal tide with shears of the large-scale flow is also possible.

6. Spatial and temporal variability

Simultaneous current meter records from the I and W1 moorings (figure 1) were analysed to show the spatial and temporal variability of the internal wavefield. Most of the moorings were positioned over relatively smooth topography at least 30 km from the nearest bank or continental shelf; however, I2 was very close to the steep Ymir Ridge, and I1 was located on the lower slope of Lousy Bank. The HKE was determined as a function of time in two frequency bands: 0.076–0.090 c/h, bracketing the semidiurnal tide but above the local inertial frequency, and 0.10–0.30 c/h, a band in the internal wave continuum everywhere below the local buoyancy frequency.

PHILOSOPHICAL TRANSACTIONS OF THE ROYAL SOCIETY A MATHEMATICAL, PHYSICAL & ENGINEERING SCIENCES

To assess the horizontal variability, the average HKE from four common depths nominally at 200, 600, 1000 and 1500 m are compared in figure 9. The average was calculated over a period of 24 days starting on 19 July, when all instruments were operating. The spectral levels determined from the GM model by appropriate integration of (2) are also shown. The local values of N determined from the average profile (figure 3) were used to scale the GM model and were assumed representative of the entire JASIN area.

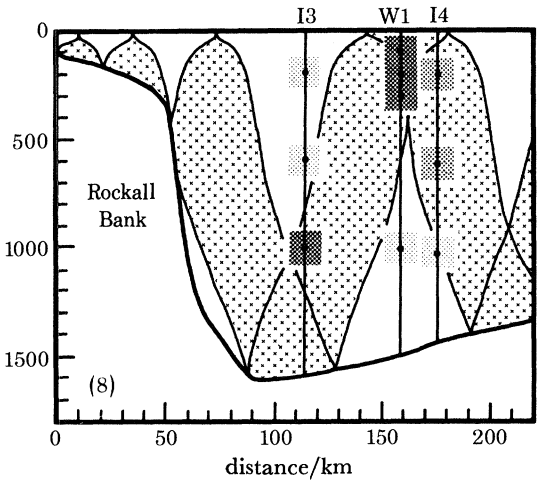

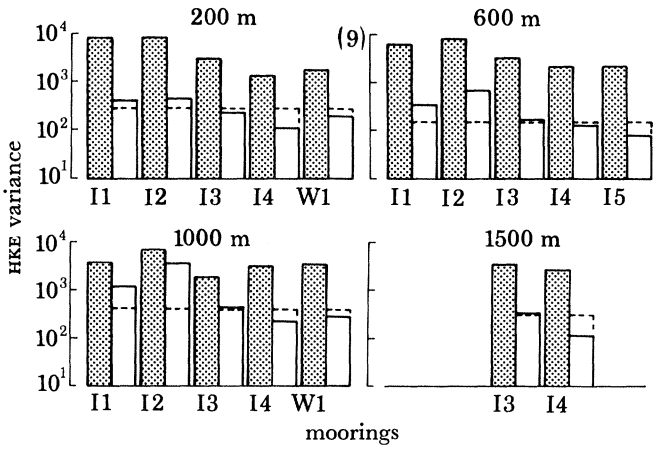

FIGURE 8. Cross section from Rockall Bank to the FIA showing the theoretical beam of internal tidal energy (shaded area between solid lines) generated at Rockall Bank (from deWitt *et al.* 1982). Tidal variance of HKE for 22–29 August measured at I3, W1 and I4 is indicated by shading; darker shading implies higher variance.

FIGURE 9. Bar graph indicating HKE in two frequency bands; 0.076–0.090 c/h (shaded) and 0.10–0.30 c/h. Spectral levels of the GM model are indicated by dashed lines.

All the measurements of the continuum spectrum over smooth topography at W1, I3, I4, and I5 agree with GM levels within a factor of three and often much better. The agreement with the GM model at I3 at all depths is remarkable; the levels at I4 are lower than GM levels. Observations near rougher topography at I1 and I2 show higher levels than the GM model. The highest levels occur at I2, located near the steep Ymir Ridge, where the continuum increases with depth to nearly ten times the GM level. Better determination of the horizontal variation of N might alter the results, but deviations from the GM levels by factors of three or more are probably significant (Briscoe, this symposium).

The semidiurnal tidal variances, which include both the barotropic and the internal tide, exhibited variability similar to that of the continuum (figure 10). At 200 and 600 m the fluctuations in the two bands were remarkably similar; the largest deviation from the average ratio of tidal to continuum variance was only 30%, while the maximum variation among the individual variance estimates was a factor of six. The correlation between the tidal and continuum variance was weakest at 1000 m over rougher topography at I1 and I2. There are several possible explanations for the observed correlation between variances in the tidal and continuum bands. Internal energy in the tidal band may cascade into the continuum through wave–wave interactions in a statistically universal fashion. This speculation is however counter to the theoretical calculations of Olbers & Pomphrey (1981), which suggest that the internal tide cannot be a significant source of energy for the continuum under the assumption of weak

interaction theory. Another possibility is that there is no cause and effect relation between the tide and continuum but that both are correlated with another quantity. One suggestion (figures 1 and 10) is that the energy levels of both the tide and the continuum vary inversely with the distance from significant topography. Further study is required to determine the nature of the link between energy in the tidal and continuum bands.

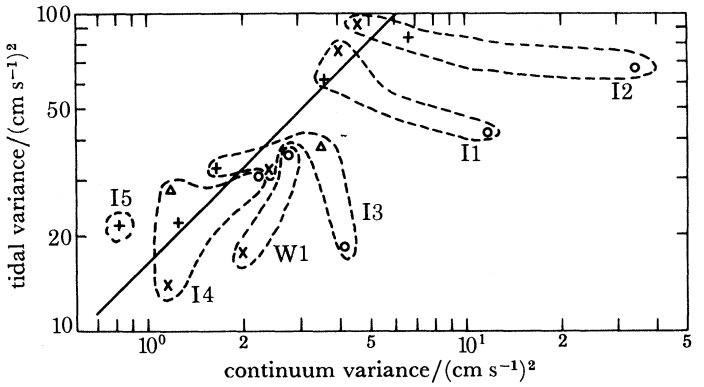

FIGURE 10. Variance of HKE in the continuum (0.1–0.3 c/h) against variance in the tidal band (0.076–0.090 c/h) from nominal depths of 200 (×), 600 (+), 1000 (O) and 1500 m (Δ). The straight line indicates a constant ratio of tidal to continuum variance fitted to data at 200 and 600 m.

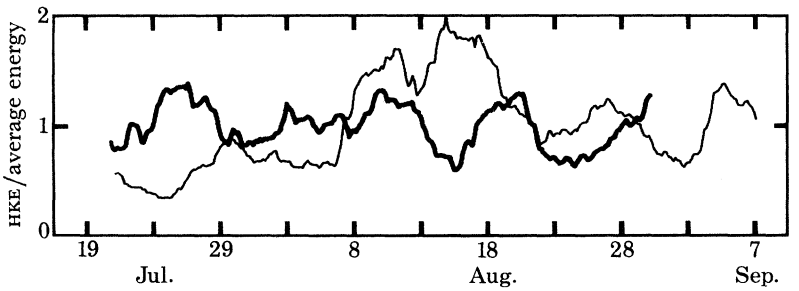

FIGURE 11. HKE in the 0.1–0.3 c/h band as a function of time from I2 at 1000 m (thin line) and I3 at 200 m (bold line). The time series are normalized by dividing by the average energy.

The temporal variations in the continuum band, 0.1–0.3 c/h, were generally rather small, normally between half and twice the average over the entire record. A typical example from I3 at 200 m is shown in figure 11. Most variability occurred at I2 at 1000 m where the HKE variance ranged from 0.3 to twice the average value over 20 days (figure 1). This instrument also showed the greatest deviation from the GM level based on the 24 day averages. A visual comparison of all the time series of HKE (continuum band) showed no apparent similarities. The separations of order 50 km horizontally and 400 m vertically were too large to relate events in one record to those in another.

To determine if any of the temporal variations were due to direct atmospheric forcing, variance of vertical displacement in the FIA at 50 m and wind variance were compared (deWitt *et al.* 1982). The correlation between wind and internal wave variance at zero lag was found to be insignificant (see also Briscoe this symposium).

PHILOSOPHICAL TRANSACTIONS OF THE ROYAL SOCIETY A MATHEMATICAL, PHYSICAL & ENGINEERING SCIENCES

7. Discussion and conclusions

The internal wavefield during JASIN was described by use of data from moored velocity and moored and towed temperature observations. The observations were examined for internal consistency and were compared with internal wave models and with results from other upper-ocean internal wave experiments.

Spectra of the mean internal wavefield at the FIA were compared with spectra from the deep ocean, as represented by the GM model. Generally, the observed spectral levels were equal to or above the GM levels, with greater differences at high frequency and wavenumber (figure 2). Exceptions occurred in the frequency spectra of displacement at 1000 m and HKE at 50 m where GM levels were twice to three times those observed even at low frequency. The shapes of the observed spectra usually agreed with the GM model only at low frequency and wavenumber. However, the observed spectral shapes in the frequency spectra of HKE at 15 m and displacement at 50 m were quite different from the GM model over the entire internal wave frequency band.

To describe the internal wave measurements at high frequency and wavenumber in JASIN, a model composed of three statistically independent modes was constructed. It was assumed that the total vertically integrated energy was partitioned among the first, second and third modes in the proportions 0.4, 0.4, 0.2, respectively. The use of modes higher than the third would violate the linearity assumption because horizontal phase speeds would then compare with the speeds of the low frequency, quasi-steady flow (figure 5). The total energy in the three modes was adjusted at each frequency to fit the displacement spectrum from B1 at 50 m exactly. The three-mode model was then compared with other measured spectral quantities.

Observed spectral features at high frequency and wavenumber that were better represented by the three-mode model than by the GM model include:

(i) The shape and level of the frequency spectra of displacement at 1000 m and HKE at 15 m (figure 2).

(ii) The details of the spectral shapes of HKE at 50 and 200 m. The levels of the three-mode model above 1 c/h agreed much better with observations than the GM model. The sharp spectral cut-off at local N predicted by the GM model was not observed at 200 m (figure 2).

(iii) The shoulder in the displacement wavenumber spectrum at high wavenumber (figure 2c).

(iv) The high vertical coherence at high frequency (0.5–3.0 c/h) and wavenumber ($0.4 \times 10^{-3} - 3.0 \times 10^{-3}$ c/m) (figure 4). The observed non-zero phase spectrum of velocity at high frequency for vertical separations is inconsistent with the GM model.

The greatest failure of the three-mode model occurred in the HKE at 1000 m where the observed high frequency levels are significantly above the model levels. Another weakness of the model is the assumption of statistical independence of the three modes. Energy exchange and hence correlation is likely between two modes that have nearly the same frequency and wavenumber (figure 5). Incorporation of this phenomena, first discussed by Eckart (1961), would significantly modify the model.

The semidiurnal internal tide represents a significant portion of the total internal wave variance. For a one-week period in August a detailed analysis of the internal tide was possible in the FIA because of the high coherence among the B moorings (figure 7). During this period the tide can be described locally as a plane wave of mode three with wavelength 36 km travelling

PHILOSOPHICAL TRANSACTIONS OF THE ROYAL SOCIETY A MATHEMATICAL, PHYSICAL & ENGINEERING SCIENCES

from Rockall Bank. The spatial variability of the HKE from moorings in the area is consistent with the beam-like structure of the internal tide generated from Rockall Bank (figure 8). The large temporal variations of internal tidal energy may be caused by changes in shear and fronts associated with mesoscale features. These changes would shift the high energy beam and would result in modulation of tidal energy observed at a fixed location. This shifting of beams from all possible topographic sources of internal tide might explain the complicated spatial and temporal variations observed throughout the JASIN area.

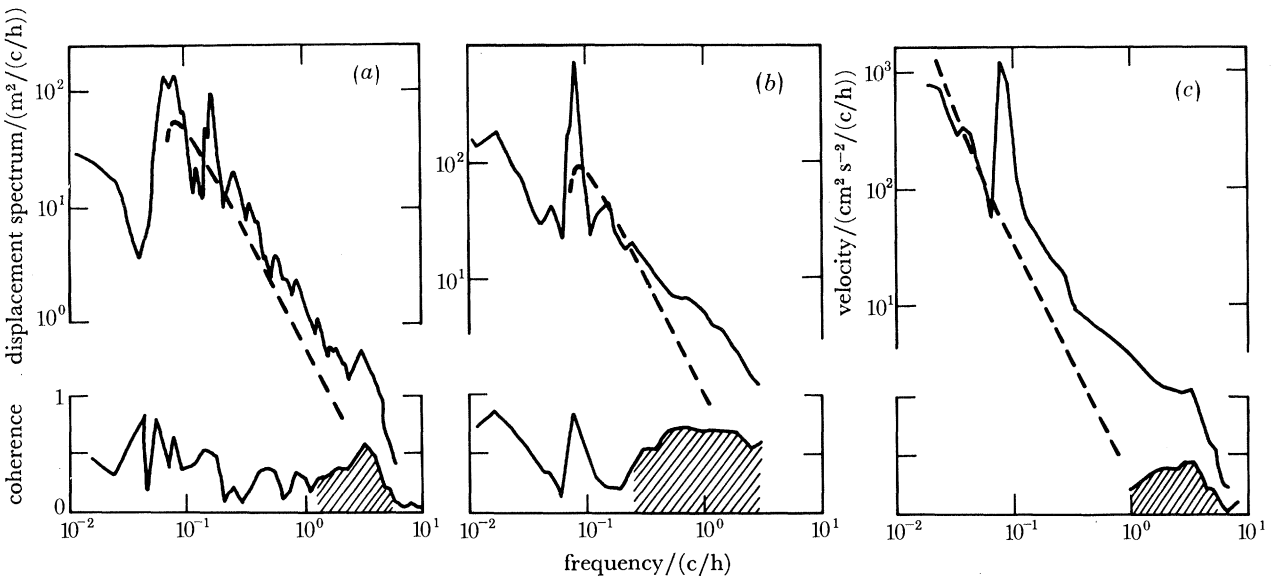

FIGURE 12. Observed frequency spectra along with vertical coherences from (*a*) MILE, (*b*) JASIN, and (*c*) GATE. Garrett–Munk spectra based on local average N are shown by the dashed lines. Displacement spectra from JASIN and MILE are from 50 and 41 m respectively; the clockwise rotary velocity spectrum from GATE is from 56 m. Coherences are from depths between 45 and 60 m (JASIN), 41 and 175 m (MILE), and 7 and 51 m (GATE); coherences that are significantly non-zero at the 95% confidence limit are shaded.

The temporal and spatial variability of HKE in the internal wave continuum band was also assessed. There was generally good agreement between the 24 day average variance in the frequency band 0.1–0.3 c/h and the expected GM levels in measurements over smooth topography (figure 9). Over rougher topography the observed levels were always above GM levels; the greatest deviation was ten times the GM level at I2 at 1000 m. Temporal fluctuations of the internal wave energy in the continuum were usually within half to twice the mean. The largest variation in time occurred at I2 at 1000 m where the highest average values were found (figure 11). There was no obvious correlation between the internal wave energies at vertical separations of 400 m and horizontal separations greater than 50 km. No correlations of internal wave energy fluctuations with the surface wind were found, even at 50 m, implying that the wind is not a significant source or that dissipation processes damp the response, thereby masking any correlation.

The frequency band 0.076–0.090 c/h containing the energetic semidiurnal tide also exhibited significant spatial variation. There is good correlation between the average levels of the tidal and continuum bands especially at 200 and 600 m (figure 10). Further investigation is required to determine whether this correlation is caused by a dynamical link between the tide and the continuum.

Upper-ocean internal wave spectra measured at JASIN have many characteristics in common with other observations from the upper ocean. Frequency spectra and vertical coherences from JASIN are compared with similar observations from MILE (Levine *et al.* 1982) and GATE (Käse & Siedler 1980) in figure 12. Observations during GATE were from the equatorial Atlantic; MILE was conducted near 50° N, 145° W in the northeast Pacific. Spectra from all three experiments agree with the GM levels at low frequency when scaled by the average local values of N, 12.5 c/h for MILE, 11.5 c/h for GATE and 8 c/h for JASIN. Additional examples of upper-ocean spectra having levels equal or greater than the GM levels are presented by Roth *et al.* (1981). The deviations from the GM model occur in a high frequency band marked by a spectral shoulder and high vertical coherences. This frequency band in JASIN (0.5–3.0 c/h) is lower in frequency than in GATE and MILE (2–5 c/h). This difference appears to be related to differences in the N profiles; the trapping of vertical modes in the upper ocean begins at lower frequency in JASIN than in GATE or MILE because of the large subsurface minimum in the buoyancy frequency in JASIN (figure 3). Although the low frequency energy appears to scale with local N, the spectral cut-off at high frequency, also indicated by a sharp drop in coherence, does not. One explanation is that as frequency is increased, the free waves are trapped in smaller vertical scales. Hence their phase speeds decrease and the likelihood of nonlinear interactions that could destroy these waves increases. This explanation is consistent with the cut-off observed at a lower frequency in JASIN than in MILE or GATE.

This research is supported by: the Office of Naval Research under contracts N00014-79-C-0004 (M.D.L. and C.A.P.) and N00014-76-C-0197 (M.G.B. and R.A.W.), the National Science Foundation under grant OCE77-25803 (M.G.B. and R.A.W.), and the Deutsche Forschungsgemeinschaft (H.P.).

References

Baines, P. G. 1974 The generation of internal tides over steep continental slopes. *Phil. Trans. R. Soc. Lond.* A **277**, 27–58.

Baumann, R. J., Paulson, C. A. & Wagner, J. 1980 Towed thermistor chain observations in JASIN. Data report 80, reference 80–14, School of Oceanography, Oregon State University.

Desaubies, Y. J. F. 1976 Analytical representation of internal wave spectra. *J. phys. Oceanogr.* **6**, 976–981.

deWitt, L. M., Bottero, J., Burt, W. V., Paulson, C. A. & Simpkins, J. 1980 Moored temperature observations in JASIN. Data report 83, reference 80–15, School of Oceanography, Oregon State University.

deWitt, L. M., Levine, M. D. & Paulson, C. A. 1982 Internal waves in JASIN: spectra, variability and internal tide. *J. phys. Oceanogr.* (Submitted.)

Eckart, C. 1961 Internal waves in the ocean. *Physics Fluids* **4**, 791–799.

Garrett, C. J. R. & Munk, W. H. 1972 Space–time scales of internal waves. *Geophys. Fluid. Dyn*, **2**, 255–264.

Garrett, C. J. R. & Munk, W. H. 1975 Space–time scales of internal waves: a progress report. *J. geophys. Res.* **80**, 291–297.

Garrett, C. & Munk, W. H. 1979 Internal waves in the ocean. *A. Rev. Fluid Mech.* **11**, 339–369.

Gould, W. J., Cutler, A. N. & Weddell, D. 1983 Long term current measurements in the N. Rockall Trough. Internal report, Institute of Oceanographic Sciences, Wormley. (In preparation.)

Gregg, M. C. & Briscoe, M. G. 1979 Internal waves, finestructure, microstructure, and mixing in the ocean. *Rev. Geophys. Space Phys.* **17**, 1524–1548.

Hendershott, M. C. 1981 Long waves and ocean tides. In *Evolution of physical oceanography* (ed. B. A. Warren & C. Wunsch), pp. 292–341. Cambridge, Massachusetts: MIT Press.

Käse, R. H. & Siedler, G. 1980 Internal wave kinematics in the upper tropical Atlantic. *Deep-Sea Res.* suppl. I, vol. **26**, 161–189.

Katz, E. J. & Briscoe, M. G. 1979 Vertical coherence of the internal wave field from towed sensors. *J. phys. Oceanogr.* **9**, 518–530.

Levine, M. D., de Szoeke, R. A. & Niiler, P. P. 1982 Internal waves in the upper ocean during MILE. *J. phys. Oceanogr.* (In the press.)

Müller, P., Olbers, D. J. & Willebrand, J. 1978 The IWEX spectrum. *J. geophys. Res.* **83**, 479–500.
Munk, W. 1981 Internal waves and small-scale processes. In *Evolution of physical oceanography* (ed. B. A. Warren & C. Wunsch), pp. 264–291. Cambridge, Massachusetts: MIT Press.
Olbers, D. J. & Pomphrey, N. 1981 Disqualifying two candidates for the energy balance of oceanic internal waves. *J. phys. Oceanogr.* **11**, 1423–1425.
Pennington, N. & Briscoe, M. G. 1979 Atlantis-II (Cruise 102) preliminary CTD data from JASIN 1978. Woods Hole Oceanographic Institution Technical report WHOI-79-42.
Peters, H. 1982 On the dispersion characteristics of high-frequency internal waves in a mean shear current. *Deep-sea Res.* (Submitted.)
Roth, M. W., Briscoe, M. G. & McComas, C. H., III. 1981 Internal waves in the upper ocean. *J. phys. Oceanogr.* **11**, 1234–1247.
Tarbell, S., Briscoe, M. G. & Weller, R. A. 1979 A compilation of moored current meter and wind recorder data. Woods Hole Oceanographic Institution Technical report WHOI-79-65.
Willebrand, J., Müller, P. & Olbers, D. J. 1977 Inverse analysis of the trimoored internal wave experiment (IWEX). Berichte 20*a* Institüt für Meereskunde an der Universität Kiel.
Wunsch, C. 1976 Geographical variability of the internal wave field: a search for sources and sinks. *J. phys. Oceanogr.* **6**, 471–485.
Wunsch, C. & Webb, S. 1979 The climatology of deep ocean internal waves. *J. phys. Oceanogr.* **9**, 235–243.

Discussion

H. M. Van Aken (*Instituut Meteorologie en Oceanografie, Rijksuniversiteit, Utrecht, Princetonplein* 5, *Utrecht* 2506 *Netherlands*). I have calculated vertical wavenumber spectra (*DS*) for the vertical displacement and I have found a β^{-3} behaviour for the wavenumber band $\beta = 1$ cycle per 500 m to $\beta = 1$ cycle per 50 m. The variance of the vertical displacement in this wavenumber appeared to be proportional to the buoyancy period. Do these results agree with your vertically standing modes model?

M. D. Levine. The scaling of the variance in a vertical wavenumber band with the buoyancy frequency is a consequence of using the WKB description of the vertical dependence of the wavefield and applies only when the vertical wavelengths are small compared with variations in the N profile (Munk 1981). It is difficult to compare Dr Van Aken's results directly with the standing mode model at high frequency where the WKB approximation is not valid and the vertical dependence of the wavenumber is best described by standing modes rather than vertical wavenumbers. Since the vertical mode shapes are a function of frequency, further analysis would be necessary to determine the connection with the vertical wavenumber spectrum.

J. M. Huthnance. (*Institute of Oceanographic Sciences, Bidston Observatory, Birkenhead, Merseyside L*43 7*RA, U.K.*). The station showing least departure from the Garrett–Munk internal wave spectrum appears to show rather regular temporal fluctuations of internal wave energy. Are these related to any other features, e.g. modulated tidal currents?

M. D. Levine. The somewhat periodic fluctuations (10–15 day period) of the HKE measured at I3 at 200 m (figure 11, bold line) are marginally significant. Similar oscillations were not always measured at the other instruments, and there is no obvious correlation among the time series even between instruments on the same mooring. No attempt has been made to relate this feature to tidal modulation.

G. Siedler (*Institut für Meereskunde, Düsternbrooker Weg* 20, *D*-2300 *Kiel, F.R.G.*). How were the energy levels determined in the Garrett–Munk model spectra that have been used as reference spectra in this study?

PHILOSOPHICAL TRANSACTIONS OF THE ROYAL SOCIETY A MATHEMATICAL, PHYSICAL & ENGINEERING SCIENCES

M. D. Levine. The Garrett–Munk spectral levels are plotted for an r-value of 190 m^2 c/h based on IWEX data as cited by Roth *et al.* (1981). Desaubies (1976) observes that the variation of r between different experiments seems to be within a factor of two. Choosing a different r would simply shift all plotted Garrett–Munk spectra by a constant factor (see equations (1)–(3)).

E. D. R. Shearman (*Department of Electronic and Electrical Engineering, University of Birmingham, P.O.* 363, *Birmingham* B15 2*TT*, *U.K.*). Were any observations of individual internal wave events made during JASIN? Internal waves in the atmosphere occur from such sources as mountain lee-waves and it would be of interest to know whether corresponding effects have been identified in the sea when tidal currents flow over topographical features.

M. D. Levine. Generators of internal waves associated with seamounts and continental shelves have been observed many times in the ocean. The most striking evidence comes from satellite synthetic-aperture radar (SAR) observations (see for example Haury *et al.* 1979; Vesecky & Stewart 1982). Similar features in the JASIN area have also been observed by Seasat (Fu & Holt 1981). Indirect evidence of generation of internal waves from the interaction of barotropic tide with topography are presented in § 5.

References

Fu, L.-L. & Holt, B. 1981 *Atlas of the Seasat synthetic-aperture radar images*. JPL publication 81–120, Jet Propulsion Laboratory, Pasadena.

Haury, L. R., Briscoe, M. G. & Orr, M, H. 1979 *Nature, Lond.* **278**, 312–317.

Vesecky, J. F. & Stewart, R. H. 1982 *J. geophys. Res.* **87**, 3397–3430.

PHILOSOPHICAL TRANSACTIONS OF THE ROYAL SOCIETY A MATHEMATICAL, PHYSICAL & ENGINEERING SCIENCES